THE JOURNAL OF BIOLOGICAL CHEMISTRY VOL. 284, NO. 15, pp. 10110–10119, April 10, 2009


# Three-dimensional Structure of $A_1A_0$ ATP Synthase from the Hyperthermophilic Archaeon *Pyrococcus furiosus* by Electron Microscopy*[S]

Received for publication, November 7, 2008, and in revised form, January 9, 2009 Published, JBC Papers in Press, February 8, 2009, DOI 10.1074/jbc.M808498200

**Janet Vonck**[‡1], **Kim Y. Pisa**[§], **Nina Morgner**[¶], **Bernhard Brutschy**[¶], **and Volker Müller**[§]

*From the* [‡]*Max-Planck-Institute of Biophysics, Max-von-Laue-Strasse 3, D-60438 Frankfurt am Main, Germany and* [§]*Molecular Microbiology & Bioenergetics, Institute of Molecular Biosciences, and* [¶]*Microkinetic, Clusterchemistry, Mass- and Laserspectroscopy, Institute of Physical and Theoretical Chemistry, Goethe University, Max-von-Laue-Strasse 9, D-60438 Frankfurt am Main, Germany*

**The archaeal ATP synthase is a multisubunit complex that consists of a catalytic $A_1$ part and a transmembrane, ion translocation domain $A_0$. The $A_1A_0$ complex from the hyperthermophile *Pyrococcus furiosus* was isolated. Mass analysis of the complex by laser-induced liquid bead ion desorption (LILBID) indicated a size of 730 ± 10 kDa. A three-dimensional map was generated by electron microscopy from negatively stained images. The map at a resolution of 2.3 nm shows the $A_1$ and $A_0$ domain, connected by a central stalk and two peripheral stalks, one of which is connected to $A_0$, and both connected to $A_1$ via prominent knobs. X-ray structures of subunits from related proteins were fitted to the map. On the basis of the fitting and the LILBID analysis, a structural model is presented with the stoichiometry $A_3B_3CDE_2FH_2ac_{10}$.**

Archaea produce ATP by an ATP synthase that is distinct from the well known $F_1F_0$-type ATP synthase occurring in bacteria, mitochondria, and chloroplasts. The A-type ATP synthases are more closely related to vacuolar (V-type) ATPase, which, however, is functionally different and acts as an ATP-driven ion pump (1). Some bacteria also harbor A-type ATP synthases, probably acquired by horizontal gene transfer (2, 3).

Like $F_1F_0$ ATP synthases and $V_1V_0$ ATPases, $A_1A_0$ ATP synthases consist of a soluble enzymatic head in the cytoplasm and a transmembrane ion-translocating domain, forming a pair of coupled rotary motors. There is clear homology in the main catalytic subunits of all types, showing a common evolutionary origin, but many of the peripheral subunits are unique for the distinct groups. The A- and V-type enzymes are considerably larger than the F-type (1).

The catalytic heads are made up of three A and three B subunits, where A is the catalytic subunit equivalent to F-type $\beta$. The A subunit contains a 90-amino acid insert near the N terminus, known as the non-homologous region, which makes this subunit with ≈66 kDa considerably larger than its homologues (4–7). The central stalk consists of the C, D, and F subunits, and the D subunit is thought to be the equivalent of the $\gamma$ subunit, responsible for conformational changes in the nucleotide-binding pockets upon rotation (8, 9). The transmembrane domain contains a rotor of a number of identical *c*-subunits and part of the *a*-subunit. The *a*-subunit is large, comprising a transmembrane domain with seven to eight predicted transmembrane helices and a soluble domain, which probably forms part of the stator. In addition, the A-type ATP synthases contain subunits H and E (10).

Structural information on the A-type and V-type ATPases has been forthcoming in recent years. For several subunits, x-ray structures have been determined, including isolated archaeal A (11) and B (12) subunits, the E subunit (13), and a bacterial A-type C subunit (14, 15). The archaeal F subunit has been solved by NMR spectroscopy (16), and the shape of an H subunit dimer is known from small angle x-ray scattering (17). Information about the whole complex has been provided by single particle electron microscopy. A first projection structure of an $A_1A_0$ ATP synthase was presented for the enzyme from *Methanocaldococcus jannaschii* (18), which revealed the $A_1$ domain, the $A_0$ domain, the central stalk, and two peripheral stalks connected by a collar near the membrane. A three-dimensional map of the ATP synthase from *Thermus thermophilus*, which although bacterial in origin is homologous to archaeal ATP synthase and, therefore, referred to as A-type ATP synthase, shows the presence of two peripheral stalks also connected by a collar near the membrane (19). Several three-dimensional reconstructions of V-type ATPases have been presented (20–22) showing up to three peripheral stalks. The heads of A-type and V-type ATPases are clearly distinguishable from F-type because of the presence of the non-homologous region of the A subunit, which forms a prominent spike near the top of the head (19, 23).

The *c*-subunits of archaea, like the *c*-subunits of F- and V-type ATPases, contain $\alpha$-helical hairpins. In most species, they have a single hairpin, like the F-type ATP synthases, but some have undergone gene multiplications. Thus, there are two-hairpin subunits in *Methanothermobacter thermoautotrophicus* (24), *Methanosphaera stadtmanae* (25), and in *Pyrococcus furiosus*, three in *M. jannaschii* and even 13 in *Methanopyrus kandleri* (26–28), showing that the number of subunits per ring varies, as in F-type ATPases where rings with 10–15 have been found (29–35). Moreover, whereas most spe-

* This work was supported by the Deutsche Forschungsgemeinschaft (SFB 472, to V. M. and Werner Kühlbrandt).

[S] The on-line version of this article (available at http://www.jbc.org) contains supplemental Fig. S1.

*The three-dimensional EM map has been deposited in the EM Data Base (http://www.ebi.ac.uk/mds/index.html) with the accession number EMD-1542.*

[1] To whom correspondence should be addressed: Max-Planck-Institute of Biophysics, Max-von-Laue-Str. 3, D-60438 Frankfurt am Main, Germany. E-mail: janet.vonck@mpibp-frankfurt.mpg.de.

cies have retained an ion-translocating glutamate in every hairpin, *M. jannaschii* has lost it in the first of three and *P. furiosus* has lost it in the first of its two hairpins. Therefore, *P. furiosus* has a typical V-type *c*-subunit that was always seen as the reason for the inability of the V-type ATPases to synthesize ATP (36–38). However, the $A_1A_0$ ATP synthase from *P. furiosus* functions as ATP synthase *in vivo* (39). The structural basis for its ability to synthesize ATP despite the V-type *c*-subunit is unknown but might reside in the $A_0$ domain and may be based on a much larger *c*-ring (40).

We have recently enriched the A-type ATP synthase from the hyperthermophilic archaeon *P. furiosus* and shown that it uses $Na^+$ as a coupling ion (41). Here, we have improved the purification protocol and purified the entire complex. We present the three-dimensional structure of the complex by electron microscopy as well as a mass analysis by laser-induced liquid bead ion desorption mass spectrometry (LILBID-MS).[2] Based on the results of these two methods, we propose a model for the subunit composition and a solution for the enigma of ATP synthesis.

## EXPERIMENTAL PROCEDURES

*Organism—P. furiosus* DSM 3638 was obtained from the Deutsche Sammlung für Mikroorganismen und Zellkulturen, Braunschweig, Germany. For purification of the ATPase, *P. furiosus* was grown in a 300-liter fermentor at 98 °C as described before (41). The pellets were stored at −80 °C.

*Purification of the $A_1A_0$ ATP Synthase of P. furiosus*—10–20 g of cells were resuspended in buffer containing 25 mM Tris, pH 7.5, 5 mM $MgCl_2$, 0.1 mM PMSF, and 0.1 mg of DNase per ml. After homogenization, the cells were disrupted by three passages through a French pressure cell at 1200 psig. Cell debris was removed by centrifugation (11,000 × *g*; 30 min). Membranes were recovered from the extract by centrifugation (12,000 × *g*; 16 h) and were washed in 100 mM HEPES (pH 7.5), 5 mM $MgCl_2$, 10% glycerol (v/v), 100 mM NaCl, and 0.1 mM PMSF (14,000 × *g*, 6 h). The supernatant after this wash step contained negligible ATP hydrolysis activity. The washed membrane pellet was resuspended in 15–20 ml of membrane buffer containing 100 mM HEPES, pH 7.5, 5 mM $MgCl_2$, 10% glycerol (v/v), and 0.1 mM PMSF. The protein concentration was determined as described (42, 43).

Membrane proteins (29 mg/ml, 16 ml) were solubilized with Triton X-100 at a concentration of 3% (v/v) (1 g of detergent/1 g of membrane protein). After 2 h of occasional mixing at 40 °C, the membranes were solubilized overnight at room temperature on a shaker.

The supernatant was collected by centrifugation (120,000 × *g*; 1 h). After $MgCl_2$ was added to the supernatant to a final concentration of 50 mM, the ATP synthase was further purified by polyethylene glycol 6000 (4.1%, wt/wt) precipitation, where contaminating proteins were precipitated. The precipitate was removed by centrifugation (120,000 × *g*; 1 h), and the pellet contained negligible ATP hydrolysis activity. The supernatant was applied to a 20–66% sucrose gradient and centrifuged for 19 h in a vertical rotor at 153,000 × *g* 4 °C (Beckman L100K, VTi 50 rotor). Samples containing the highest ATP hydrolysis activity (determined as described in Pisa *et al.*, Ref. 41) were pooled and applied to anion exchange chromatography (DEAE-Sepharose), equilibrated with 100 mM Tris, pH 7.5, 5 mM $MgCl_2$, 10% glycerol (v/v), 0.1% Triton X-100, and 0.1 mM PMSF.

Elution was performed with a salt gradient from 0 to 1 M KCl in 100 mM Tris, pH 7.5, 5 mM $MgCl_2$, 10% glycerol (v/v), 0.1% Triton X-100, and 0.1 mM PMSF. The ATPase-active fractions were pooled and concentrated on Vivaspin 20-ml (Biofiltronic GmbH, Nörten-Hardenberg, Germany) 100-kDa concentrators. The concentrated sample was loaded on a Superose 6 column (10/30 Amersham Biosciences) and eluted with 50 mM Tris-HCl, pH 7.5, 5 mM $MgCl_2$, 10% glycerol (v/v), 50 mM KCl, 0.1% Triton X-100, 0.1 mM PMSF. The peak fractions were analyzed by SDS-PAGE. All steps were performed at 4 °C.

*Tryptic Digest and MALDI-TOF Analysis*—The products of the $A_1A_0$ ATPase were excised from a gel and subjected to in-gel digestion protocols and MALDI-TOF analysis as described (41).

*LILBID-MS*—The $A_1A_0$ ATPase protein was buffer-exchanged and concentrated to a final concentration of 3 μM in 10 mM ammonium acetate with 0.05% dodecylmaltoside (DDM) with Microcon filters (Microcon YM-100, Millipore GmbH Schwalbach/Ts. Germany). LILBID-MS of the sample was performed as described previously (44, 45). Briefly, microdroplets (50-μm diameter; volume, 65 pl) of the sample solution was introduced into vacuum by an on-demand, piezo-driven droplet generator at a frequency of 10 Hz. There the droplets are irradiated one by one by IR laser pulses, tuned to the absorption maximum of water at around 3 μm. The laser energy is transferred into the liquid via excitation of the stretching vibrations of water, inducing an instantaneous transition into the supercritical state of the liquid. There the droplets explode and the charged biomolecules from solution are set free. Because of the loss of solvent screening in this process, most of the ions in solution are neutralized and only 1 in 10,000 escape into vacuum, called "lucky survivors." These are accelerated and mass-analyzed in a home-built time-of-flight (TOF) reflectron mass spectrometer, equipped with a custom-built high mass ion-detector. The spherical isotropic explosive expansion of the ion cloud (with a velocity of around 800 m/s) limits the present resolving power in the kilodalton mass range to an approximate M/ΔM value of 100 and even lower in the higher mass range.

*Electron Microscopy (EM) and Image Analysis*—The $A_1A_0$ sample was applied to glow-discharged carbon films and negatively stained with 1% (w/v) uranyl acetate. Electron micrographs were collected using a Philips CM120 (FEI, Eindhoven, the Netherlands) at an accelerating voltage of 120 kV under low dose conditions. Images were taken at a magnification of ×44,000 on Kodak SO-163 electron image film. The negatives were developed for 12 min in full-strength D-19 developer. Negatives checked by optical diffraction for correct defocus and lack of drift and astigmatism were digitized on a PhotoScan scanner (Z/I Imaging, Aalen, Germany) at a pixel size of 7 μm. Subsequently, adjacent pixels were averaged to yield a pixel size

[2] The abbreviations used are: LILBID, laser-induced liquid bead ion desorption; EM, electron microscopy; MS, mass spectroscopy; MALDI, matrix-assisted laser desorption/ionization; TOF, time-of-flight; PEG, polyethylene glycol; PDB, Protein Data Bank; PMSF, phenylmethylsulfonyl fluoride.

**TABLE 1**
**Purification of the $A_1A_0$ ATP synthase of *P. furiosus***

| Purification step | Protein | ATPase activity | Specific activity | Enrichment | Yield |
|---|---|---|---|---|---|
| | *mg* | *unit* | *milliunit/mg* | *fold* | *%* |
| Membranes | 335 | 106 | 300 | 1 | 100 |
| TX-100 supernatant | 66 | 60 | 900 | 3 | 56.6 |
| PEG 6000 supernatant | 64 | 67 | 1100 | 4 | 63.4 |
| Sucrose gradient | 3.1 | 76.8 | 24600 | 78 | 72.4 |
| DEAE column conc. | 1 | 5.1 | 6000 | 19 | 4.8 |
| Gel filtration | 0.3 | 2 | 6500 | 20.5 | 1.8 |

on the specimen of 4.77 Å. 12,912 particle images were selected using the boxer program from EMAN (46). Images were processed using Imagic V (47). Briefly, images were band pass-filtered, aligned translationally and rotationally, and subjected to multivariate statistical analysis and classification. Images assigned to the same class were averaged. As all classes represented views along the long axis of the molecule, for three-dimensional reconstruction an initial model was created by assigning angles to some class averages and creating a volume in Imagic. The model was iteratively refined by the standard refine command of EMAN (46). To estimate the resolution of the final map the Fourier shell correlation between two maps calculated from half of the particle images each was determined by the EMAN routine *eotest*. Three-dimensional visualization and fitting of x-ray structures into the map was done by UCSF Chimera (48).

## RESULTS

*Purification and Characterization of the $A_1A_0$ ATP Synthase of P. furiosus*—The $A_1A_0$ ATP synthase preparation studied previously lacked the subunits F and H and contained an AAA ATPase (thermosome) as a major contaminant (41). The thermosome, which has a calculated molecular mass around 900 kDa, was clearly visible in electron micrographs and easily distinguishable from the $A_1A_0$ ATP synthase. The new protocol yielded an intact enzyme and removed the thermosome (see "Experimental Procedures"). In short, the membranes were centrifuged at low speed, the enzyme was solubilized, precipitated with PEG, and further purified by sucrose density centrifugation and ion exchange chromatography followed by gel filtration. The purification is summarized in Table 1. The specific activity of various enzyme preparations ranged from 1.9 to 6.5 units/mg protein, and the overall yield was 1.8%.

The ATP synthase preparation in SDS-PAGE contained 14 polypeptides of apparent molecular masses 130, 97, 65, 60, 54, 52, 40, 30, 25, 23, 16, 12, 11, and 9 kDa (Fig. 1). Proteins were identified by MALDI-TOF analysis or MS/MS. The 130-kDa protein was identified as methylmalonyl-CoA decarboxylase subunit $\alpha$. The 97-kDa protein was identified by MALDI-TOF analysis and MS/MS in duplicate to be subunit C. No other polypeptide was found, indicating that this band represents a multimer of subunit C (42 kDa). Subunit A (65 kDa) matches exactly the mass deduced from the genome sequence. The band at 60 kDa was identified by MS/MS to contain an oligomeric form of subunit *c* and subunit *a*. The subunits could not be resolved by SDS-PAGE, neither in 8% nor in 10% gels. Furthermore, the band cross-reacts with the antiserum against subunit *a* or *c* of *M. jannaschii*. The hydrophobic character of this

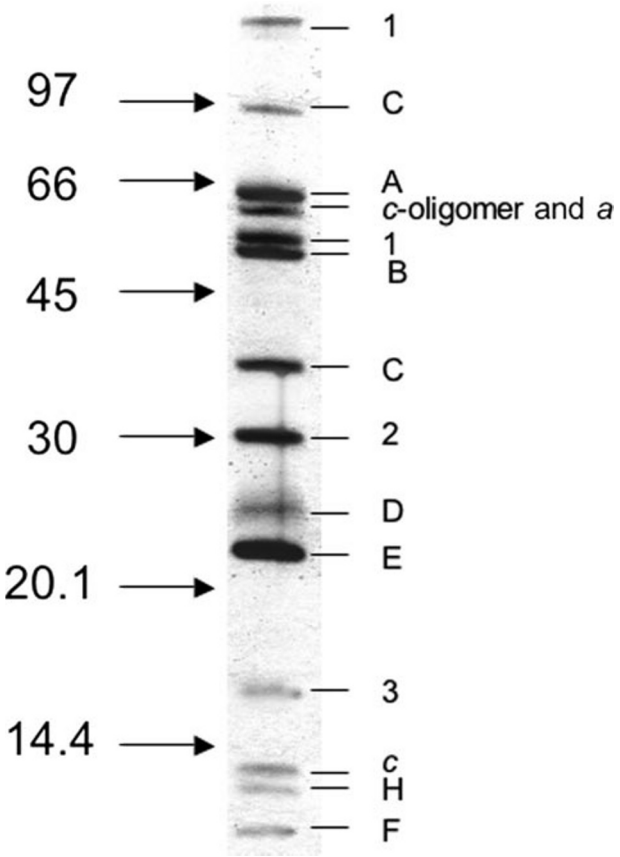


FIGURE 1. **Subunit composition of the $A_1A_0$ ATP synthase of *P. furiosus*.** The preparation was subjected to SDS-PAGE on 12.5% gels and silver-stained. A molecular mass marker is shown on the *left* and subunits on the *right*. *Letters* indicate the $A_1A_0$ subunits, and numbers the impurities: *1*, methylmalonyl-CoA decarboxylase subunit $\alpha$; *2*, not identified; *3*, hypothetical protein PF0672 (see text).

membrane protein complex makes it difficult to estimate its molecular weight on an SDS-PAGE gel. The 54-kDa protein was also identified as methylmalonyl-CoA decarboxylase subunit $\alpha$ (which has a predicted mass of 57.1 kDa). The 52, 40, 25, and 23 kDa proteins were identified as subunits B, C, D, and E. The 30-kDa protein could not be identified, and the 16-kDa protein was identified as the hypothetical protein PF0672 from the *P. furiosus* genome (49). The 12-, 11-, and 9-kDa proteins were identified as subunits *c* (monomeric form), H, and F. These data showed the absence of thermosomes in the preparation and demonstrated that all subunits deduced from the genome sequence are indeed present in the preparation.

*LILBID Analysis*—The molecular mass of the complex and its subcomplexes was determined with LILBID-MS, a recently established powerful method for the determination of subunit stoichiometries in membrane protein complexes, as has been demonstrated for the cytochrome oxidase from *Paracoccus denitrificans* (45) and $F_1F_0$ *c*-rings from different organisms (33). For the $F_1F_0$ ATP synthase from *Bacillus* sp. strain TA2.A1, all subunits have been identified by LILBID-MS (50). Fig. 2 shows the LILBID mass spectra of the *P. furiosus* ATP synthase. Soft ion desorption conditions at low laser intensity allow the complex to be transferred intact into vacuum without fragmentation. The mass spectra were calibrated against the known subunits of complex I of *Y. lipolytica*, which are in the

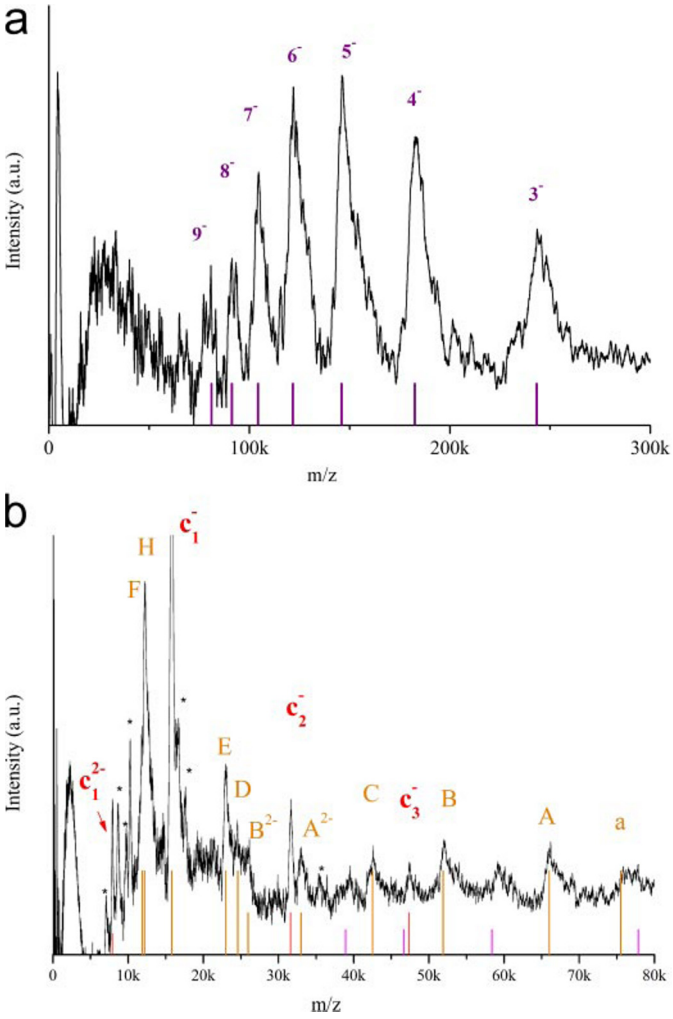


FIGURE 2. **LILBID-MS analysis of $A_1A_0$.** *a*, spectrum of the holoenzyme at low laser intensity. The *numbers* represent the different charges of the enzyme, indicating a molecular mass of 730 ± 10 kDa. *b*, upon increase of the laser intensity, the complex disintegrates into subcomplexes and individual subunits. *Orange bars* show different subunits of the complex. *Red* indicates the *c*-subunit. A series of *purple bars* at the theoretical values for an *m*/*z* distribution of the mass 233 kDa show the appearance of a subcomplex. Unassigned peaks are indicated with an *asterisk*.

same mass range (51). The mass spectrum in Fig. 2*a* shows an *m*/*z* distribution of the anionic complex with charges varying from 3 to 9. The peaks are broadened due to an increase in initial energy of the ions with higher *m*/*z*. Different from other membrane protein complexes but similar to the $F_1F_0$ ATP synthase (50), the detergent is more or less completely lost by the desorption. The reason might be an overall small percentage of solubilized surface area and less ruggedness of the hydrophobic landscape, leading to less affinity for binding and retaining detergent molecules. The overall mass, calibrated to the maximum of the ion peaks of the complex, was determined as 730 ± 10 kDa.

At harsher desorption conditions, achieved by increasing the laser intensity, the energy transferred into the system dissociates the complex partly into single subunits and subcomplexes. All masses of the subunits deduced from the genome sequence could be found in the spectra (Fig. 2*b* and Table 2). They are indicated by sticks in the spectra. Doubly charged states are

**TABLE 2**
**Theoretical and measured masses of the $A_1A_0$ ATP synthase subunits**

| Subunit | Theoretical mass | LILBID mass |
|---|---|---|
| | *Da* | *kDa* |
| A | 65,900 | 66.0 |
| B | 51,785 | 51.9 |
| C | 42,515 | 42.5 |
| D | 24,895 | 24.6 |
| E | 23,502 | 23.0 |
| F | 11,740 | 11.9 |
| H | 12,394 | 12.2 |
| *a* | 75,466 | 75.5 |
| *c* | 15,806 | 15.8 |

visible for the *c*-subunit (the most abundant subunit) and the two catalytic proteins A and B, which are also highly charged in solution. A similar observation was made for these subunits in the $F_1F_0$ ATPase (50).

One of the critical questions is whether the mature subunit *c* has indeed four transmembrane helices or whether it is post-transcriptionally or post-translationally modified. The mass calculated for subunit *c* is 15.8 kDa, and indeed, a 15.8-kDa protein was found in the complex. There is no mass found for a protein of around 8 kDa, which would have only two transmembrane helices. In addition, oligomers of *c* appear in the mass spectrum such as $c_2^-$ and $c_3^-$, indicating an incomplete fragmentation of the *c*-ring at this elevated level of laser intensity. However, an ion signal at $(c/2)_3^-$ is not observed, again indicating a *c*-subunit size of 15.8 kDa.

The spectra contained some additional peaks that could not be assigned to any of the subunits. Most of these are at low *m*/*z*, and some may arise from the 16- and 30-kDa impurities (Fig. 1). Interestingly, a series of unexpected ion signals in the higher *m*/*z* region corresponds to a mass to charge ratio of 233 kDa with charge states of −3 to −6 (*purple bars* in Fig. 2*b*). Such large complexes form broad peaks of which the onsets are measured to determine the theoretical masses. The peak around $m/z = 46{,}000$ is overlaid by a peak from $c_3$, and the peak around $m/z = 78{,}000$ with the *a* peak. The *a* peak is reproducibly very broad, therefore the assumption of an overlay with another peak seems reasonable. Among the various combinations of subunits, only an $ac_{10}$ (75 + 10 × 15.8 kDa) subcomplex would correspond to a mass of 233 kDa. This gives additional evidence, apart from the SDS-PAGE, for a stable $ac_n$ subcomplex, and indicates that the *c*-ring consists of 10 subunits.

*Electron Microscopy and Image Processing*—The *P. furiosus* $A_1A_0$ preparation was monodisperse and showed typical dumbbell-shaped particles with no hint of barrel-shaped thermosomes (Fig. 3*a*). An initial image analysis by IMAGIC V of a 7500-particle data set resulted in many different class averages with features including a head with one or more spikes, a distinct central stalk, a prominent "collar," indications of one or two peripheral stalks, and a rather large $A_0$ domain with clear substructure (Fig. 3*b*). The large number of different views precluded a reconstruction by random conical tilt, for which particles in identical orientations are needed. It suggested that the particles might represent a single-axis tilt series around the long axis of the molecule, which would contain all information necessary for a three-dimensional reconstruction. The complex was reconstructed by EMAN, which can iteratively refine a data

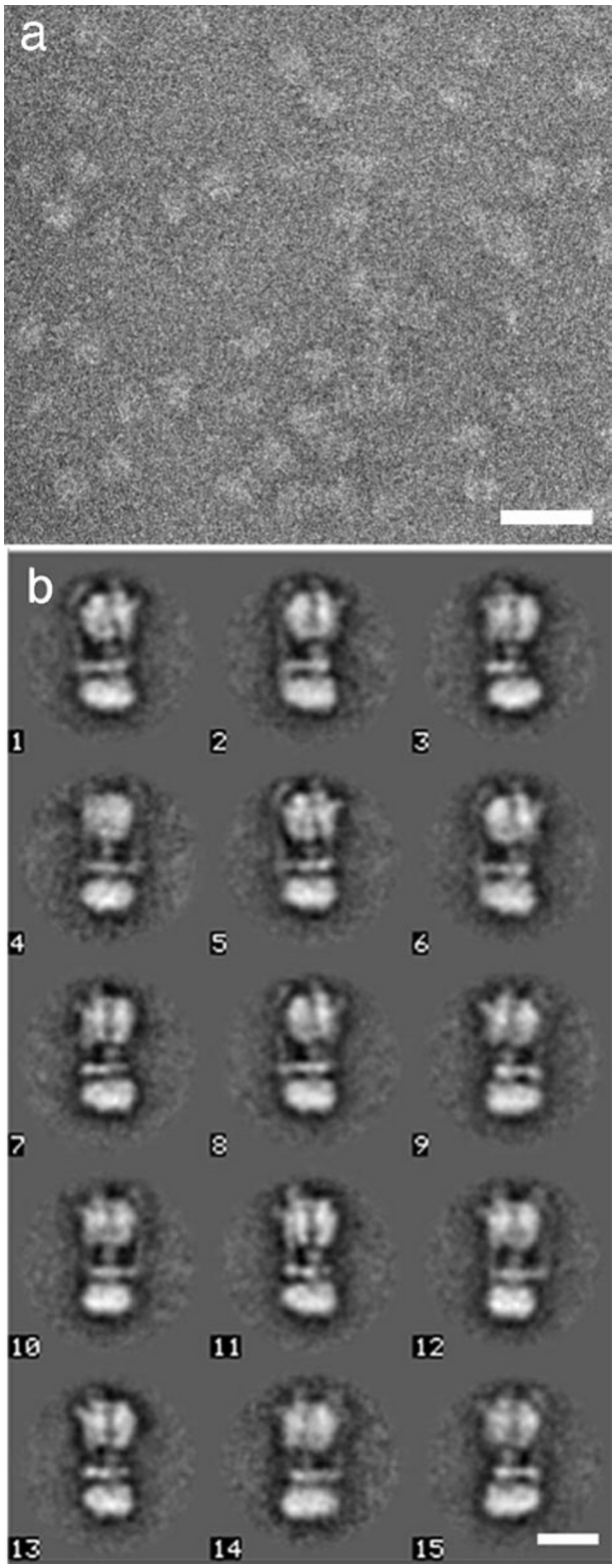


FIGURE 3. **Electron microscopy of *P. furiosus* ATP synthase.** *a*, electron micrograph of $A_1A_0$ negatively stained with uranyl acetate. The *bar* represents 25 nm. *b*, selected class averages after multivariate statistical analysis and classification.

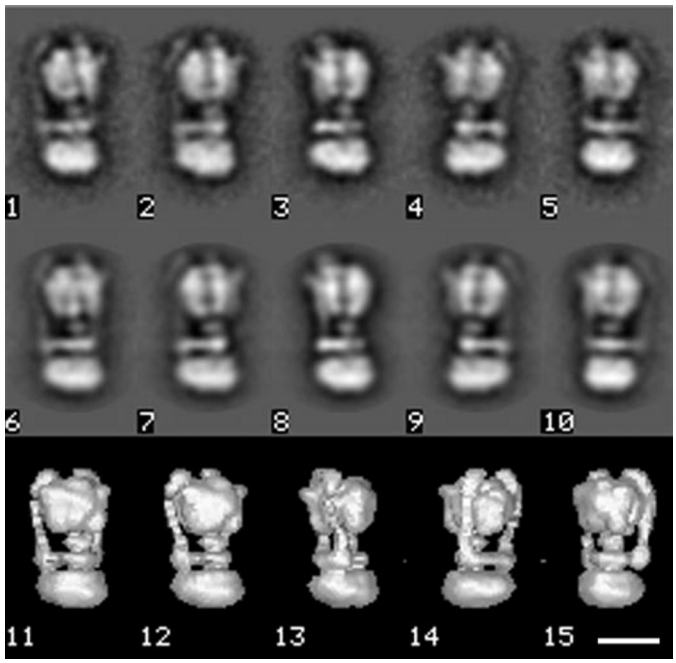


FIGURE 4. **Comparison of class averages and reprojections of the three-dimensional map.** *1–5*, selected class averages. *6–10*, reprojections of the three-dimensional map and 11–15: surface representations corresponding to the class averages. Relative projection angles are 0, 20, 80, 200, and 310° around the long axis. All images were created using IMAGIC V.

set to an initially very crude three-dimensional model (46). An initial model consisting of a large and a small domain was created by assigning azimuthal angles to some class averages. The data set was iteratively refined against this model, resulting in a clearly asymmetric structure with hints of two peripheral stalks. More data were added from particles in slightly different orientations that had initially been excluded. Refinement of this 13,000-particle data set resulted in a model with two continuous peripheral stalks. All class averages from the initial analysis by IMAGIC could be matched to one reprojection of the three-dimensional volume (Fig. 4). The relative angles of the classes that had been used in the starting model had no relation to their original assignment, showing clearly that the reconstruction process by EMAN was robust enough to overcome any bias from the starting model. The final volume was estimated to have a resolution of 23 Å by Fourier Shell Correlation (0.5 cut-off criterion). The map is shown in slices along the long axis (Fig. 5*a*), and in the perpendicular direction (Fig. 5*b*) and in a surface representation (Fig. 6). It shows a hollow head displaying six distinct densities, an asymmetric $A_0$ domain consisting of a hollow ring with a bulge on one side, a central stalk made up of two distinct domains, and a stator with two peripheral stalks, which are both connected to a collar around the central stalk while one of them is connected to the bulge on $A_0$.

*The Head*—The $A_1$ head shows pseudo-3-fold symmetry and has a strong resemblance to the isolated $A_1$ from *Methanosarcina mazei* Gö1 (23). The head shows clear asymmetry because of the presence of the central stalk. It displays a central cavity surrounded by six densities representing the three A and three B subunits, as can be seen in the sections 22–31 of Fig. 5*a*. Three of the densities have a bulge on the top, visible as "spikes" in the class averages (Fig. 4*b*), and can thus be identified as the catalytic subunits A (equivalent to $\beta$ in $F_1$), which are distinguished by a 90-amino acid insertion forming a $\beta$-sandwich (11). X-ray structures of the individual A subunit from *Pyrococcus horiko-*

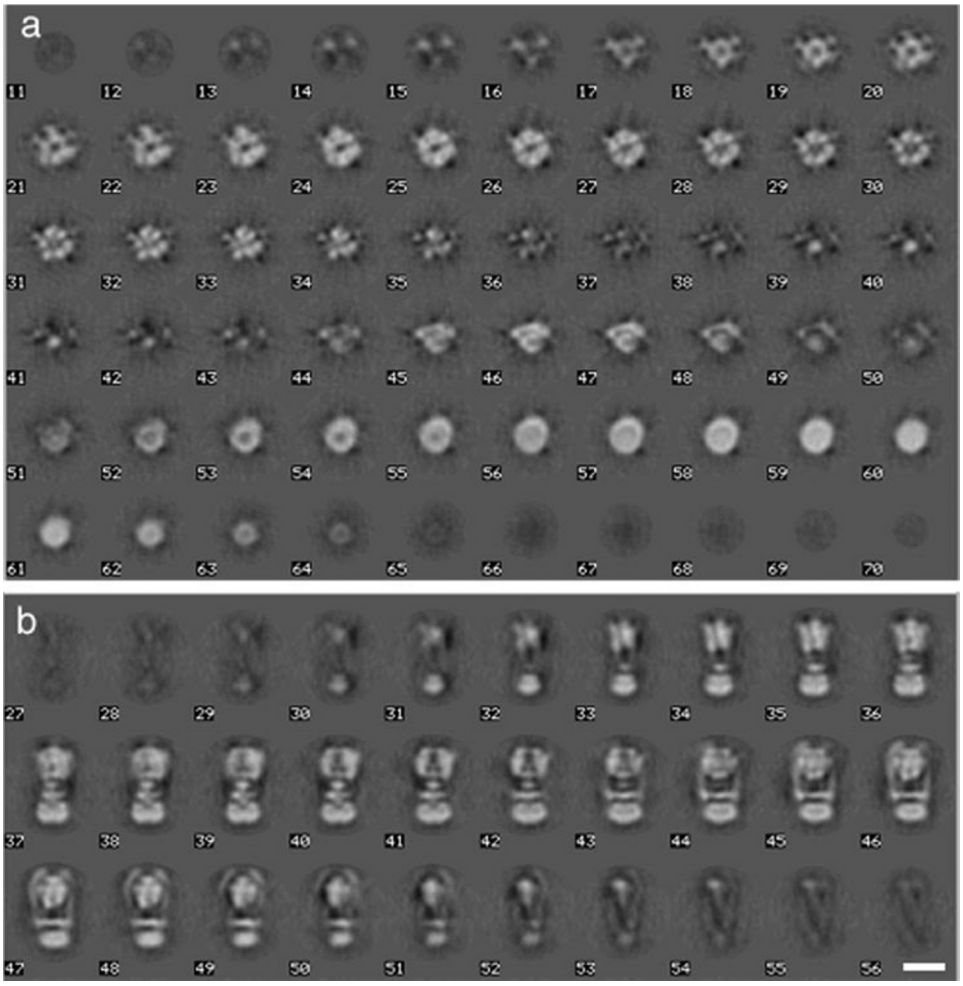


FIGURE 5. **Three-dimensional reconstruction of *P. furiosus* $A_1A_0$.** *a*, slices of the model perpendicular to the long axis. *b*, slices along the long axis. The slices are separated by 4.77 Å.

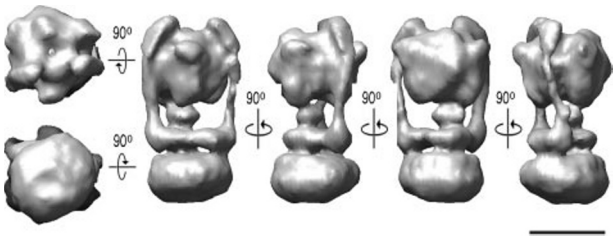


FIGURE 6. **Surface representation of the model viewed in different orientations.** The *scale bar* represents 100 Å.

*shii* (PDB 1VDZ) (11) and the B subunit from *M. mazei* Gö1 (PDB 2C61) (12) have been determined. Because of the low resolution of the model, it was not possible to fit the individual A and B subunits unambiguously. Instead, the bovine $F_1$ head (PDB 1H8E) was fitted to the EM density, and three A and three B subunits were fitted to the bovine $F_1$ subunits at the positions dictated by the presence of the bulges. The absolute handedness of the structure cannot be determined by our reconstruction procedure, so we tried the fit with both the EM structure and its mirror image. Because of the well-defined structure and asymmetry of the head, especially at the lower part where the A subunits protrude much further than the B subunits (see Fig. 7*h*), the correct handedness could be determined unambiguously, and the model fitted quite well (Fig. 7, *a*, e, *h*). It is clear that the peripheral stalks connect to the B subunits exclusively (Fig. 7*a*), as was observed for the *T. thermophilus* structure (12).

*The Central Stalk*—The central stalk descends from the head at an acentric position and attaches to the $A_0$ domain inside the ring (Fig. 5*a*, *slices 39–40*). Two distinct domains can be distinguished, a smaller, knob-like one above the collar and a larger, funnel-shaped one starting inside the collar and continuing inside the ring. The structure of the C subunit of *T. thermophilus* ATPase was solved by x-ray crystallography (14), and it was localized in the lower position of the central stalk (19, 52). This position can be clearly confirmed in the *P. furiosus* map (Fig. 7, *c*, *e*, *f*). The C subunit consists of three bundles of four α-helices each. Three domains can also be recognized in the EM density (Fig. 5*a*, *slices 45–48*). The C subunit fits very well in the stalk density, although it is not possible to distinguish the three domains (Fig. 7, *c*, *e*, *f*). The top surface is at the level of the collar and at the bottom the C subunit connects to $A_0$ inside the *c*-ring, which is hollow at this level (Fig. 7, *d–f*).

The other central stalk components are subunits D and F, with molecular masses of 25 kDa and 12 kDa, respectively. Subunit D can be cross-linked to the inside of subunit B (53) and has a high α-helical content (54). Unlike the C and F subunits, it is protected from trypsin degradation in an $A_3B_3CDF$ $A_1$ subcomplex (8); it is probably the equivalent of the γ subunit in F-ATP synthase and would thus be located inside the head. Recently an x-ray structure of the *P. furiosus* F subunit (PDB 2QAI) as well as an NMR structure of subunit F of *M. mazei* Gö1 were presented (16). Both structures show a globular domain consisting of helices and strands, with the C terminus forming a flexible extension in the NMR structure that was for the most part not visible in the x-ray map. Based on its shape, the globular domain fits well in the central stalk domain above the C subunit (Fig. 7, *b*, *e*, *f*). The C terminus can be cross-linked to B (16), so the F subunit is probably oriented with the C-terminal helix pointing toward the head and the N-terminal globular domain connecting to the C subunit. At the low resolution of the EM map, the orientation of the F subunit in the bulge cannot be determined, and the subunit has been fitted manually (Fig. 7*b*). The bulge may also be occupied by a part of the D subunit, for which there is no structure.

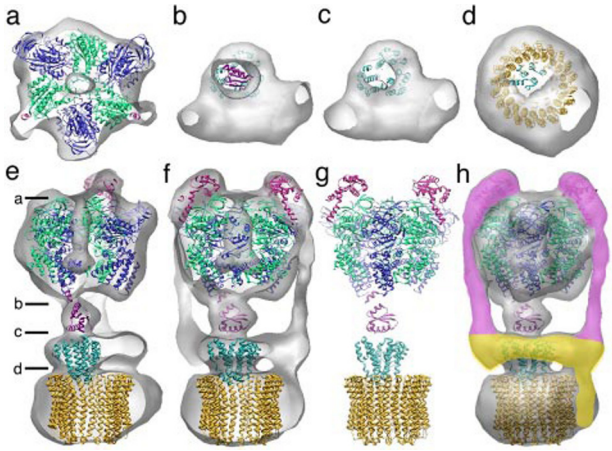


FIGURE 7. **Fitting of x-ray structures in the EM map.** *a–f*, cut-open views of the map. *a–d*, vertical views of the map, cut at the levels indicated in *e*. *a*, fitting of $A_3B_3$; A from PDB file 1VDZ (11) (*blue*) and B from 2C61 (12) (*green*). *b*, fitting of the F subunit (1QAI) (*purple*). *c*, fitting of the C subunit (*turquoise*) (1R5Z (14)). *d*, fitting of the 20-hairpin *E. hirae* A-type *c*-ring from 2BL2 (52) (*gold*). *e* and *f*, two perpendicular views along the membrane plane. The EC domain is fitted to the knobs from 2DM9 (13) (*pink*). *g*, all fitted subunits in the same orientation as *f*. *h*, model for the stator with the *a*-subunit in *yellow* and the EH dimers in *pink*. The molecular graphics images were produced using the UCSF Chimera package from the Resource for Biocomputing, Visualization, and Informatics at the University of California, San Francisco (supported by NIH P41 RR-01081).

*The $A_0$ Domain*—The *P. furiosus* $A_0$ domain has an oval shape and displays clear substructure. The cytoplasmic half is hollow, and there is a shallow indentation opposite the hole on the extracellular side (Fig. 5, *a*, *slices 52–55* and *b*, *slices 37–40*). These features are likely to represent the center of the *c*-ring. As the LILBID analysis suggested that the ring consists of ten 15.8-kDa subunits, the map density was compared with *c*-rings of known structure. Rings of various sizes ranging from 10 to 15 $\alpha$-helical hairpin subunits have been found for the $F_1F_0$ type (29, 31–35, 55). For A- and V-type, the only known stoichiometries are for the *Enterococcus hirae* ring consisting of 10 duplicated subunits, comprising 20 hairpins (52) and the *T. thermophilus* ring, which has 12 hairpins (56). Two rings have been solved by x-ray crystallography: the bacterial $F_0$ *c*-ring from *Ilyobacter tartaricus* (57) with 11 hairpins and the 20-hairpin, V/A-type *c*-ring from *E. hirae* (52). Comparison with the EM structures of the ATP synthases from *T. thermophilus* (19) and from *Bacillus* sp. TA2.A1 (58) shows that the *P. furiosus* membrane domain is larger than that of these species, which were recently shown to contain a $c_{12}$-ring (56) and a $c_{13}$-ring (33), respectively. The *I. tartaricus* $c_{11}$-ring is clearly much too small when compared with the hole in the ring (not shown), whereas the *E. hirae* ring fits quite well (Fig. 7, *b* and *h*). The hole seen in the cytoplasmic side of the *P. furiosus* ring is also present in *E. hirae*, where the other side is filled with lipid. A similar situation is likely to exist in *P. furiosus.* The *c*-subunit sequences are quite similar and like in *E. hirae*, the first and third helices, which form the inner ring, are completely hydrophobic at the N termini (facing away from $A_1$), whereas the C-terminal parts (facing $A_1$) contain several charged residues (41). This is consistent with the negative stain images, as the lipid-filled hydrophobic end would not be accessible to stain unlike the water-filled top part of the ring. We conclude that the *P. furiosus* ATP synthase has a 20-hairpin *c*-ring similar to the one in *E. hirae*.

Outside the ring, another mass is visible, which is connected to the collar (Fig. 7, *d–f*). This indicates the presence of the hydrophobic part of the *a*-subunit at this location. This subunit is predicted to have 7–8 transmembrane helices (1), which is compatible with the size of the $A_0$ density. The *a*-subunit has a large hydrophilic domain that forms part of the stator, as discussed below.

*The Stator*—Two peripheral stalks run from prominent knobs on $A_1$ to a level above $A_0$, where they are connected to each other via a collar surrounding the central stalk. The knobs are ~120° apart and connect to two B subunits, as discussed above. Unlike in the *T. thermophilus* reconstruction (19), the two knobs are not connected to each other across the $\alpha$- and $\beta$-subunits. The collar runs along the upper part of the C subunit parallel to the *c*-ring, and the collar and C subunit share a flat surface 30 Å above the $A_0$ domain. Although in the surface representation the collar and central stalk seem to be connected, a separation between these two features is visible in the EM density (Fig. 5*a*, *slices 45–49*). This separation is expected considering the rotary mechanism of the ATP synthase. One of the peripheral stalks is connected to $A_0$; the other stalk extends laterally outside the $A_0$ region and has no connection below the level of the collar.

The three subunits forming the stator are E, H, and *a*. The 12-kDa H subunit is the smallest protein in $A_1A_0$. Recently, solution x-ray scattering experiments have shown that the isolated H subunit forms a parallel dimer and has an extended "boomerang" shape with two arms of 68 and 120 Å length, respectively (17). A secondary structure prediction by PSIPRED (59, 60) for the H subunit shows an N-terminal helix of ~60 amino acids separated by a short coil region from a 40-amino acid C-terminal helix (supplemental Fig. S1*a*), which fits well to the SAXS data. The C terminus of H can be cross-linked to the N terminus of the A subunit (on top of the head) in *M. mazei* Gö1 (61), suggesting that H is part of the peripheral stalk, oriented with the C terminus on the head and the N terminus near the collar.

The 23-kDa E subunit consists of two domains, a highly helical N-terminal domain ($E_N$) and a C-terminal domain ($E_C$) with short helices and $\beta$-strands (supplemental Fig. S1*c*). The x-ray structure of the $E_C$ domain from *P. horikoshii* has recently been determined (13); it has an elongated shape ~75 Å long with $\alpha$-helical and $\beta$-strand elements and forms a tight dimer in the crystal structure, with all the predicted secondary structure elements (supplemental Fig. S1*c*). The $\alpha$-helical N-terminal domain ($E_N$) is homologous to H and to the $F_1F_0$ *b*-subunit and interacts with the H subunit (13). The equivalent E subunit in yeast V-type ATPase can be cross-linked to the full-length of the outside of the B subunit (53, 62), placing E in the peripheral stalk. A recent study shows that the E and H subunit from *Thermoplasma acidophilum*, when expressed together or reconstituted, form a stable heterodimer with high affinity (63), suggesting that the H or E homodimers formed in solution or in crystals of the isolated subunit are artifacts. This was confirmed in an EM study of the *T. thermophilus* ATPase, where antibodies against an EG complex (equivalent to EH in archaea) attached to both sides of the head, while not or weakly binding to isolated E or G (64). All this evidence places an EH dimer in

each peripheral stalk. The globular $E_C$ domain (13) has the right dimensions for the knobs on the head (Fig. 7, *e* and *f*), and the C terminus of the H subunit is also likely to reside there, as shown above. The stalks would thus be formed by heterodimers of the N-terminal domains of E and H, both of which have high α-helical propensity (supplemental Fig. S1, *b* and *c*) and are likely to form coiled-coils.

The 75-kDa *a*-subunit is the largest protein in the $A_1A_0$ complex. It has a hydrophobic C-terminal domain predicted to have 7–8 α-helices, forming the equivalent of *a* in $F_1F_0$ (1), whereas the N-terminal domain is hydrophilic. We conducted a secondary structure prediction with PSIPRED (59, 60) (supplemental Fig. S1*b*). The C-terminal 300 amino acids form the hydrophobic domain. The 360 amino acid N-terminal domain contains two long α-helices for residues 100–140 and 235–290 as well as several shorter helices, stretches of β strands and loops. The only possible location for $a_N$ is the collar connecting the two peripheral stalks, which is the only part of the three-dimensional volume not accounted for by other subunits and is also connected to the $A_0$ domain where the $a_C$ domain has been localized. Thus, the two domains of the *a*-subunit are at right angles to each other (Fig. 7*h*). A structure parallel to the membrane domain has been seen in a three-dimensional EM structure of bovine brain $V_0$ (65), supporting this interpretation.

The two peripheral stalks in this model have an identical composition, and being 120° apart on the 3-fold symmetric head, their interactions with $A_1$ via a B subunit will be identical as well. However, the symmetry breaks at their connection to the collar, which is made up of a single subunit. Close inspection of the *a*-subunit sequence (supplemental Fig. 1*a*) shows some repeating structural elements. There are two predicted long α-helices, one of ~40 amino acids (residues 100–140) and one of ~55 (235–290). At four places, there is a short predicted α-helix flanked by two β-sheets, the first at the N terminus, the second and third immediately adjacent to each other after the first α-helical stretch, and the fourth after the longest α-helix, just before the membrane domain. The first and third βαβ domain are ~28-amino acids long, and the second and fourth ~33. Interestingly, there is 33% sequence identity and more than 50% similarity between the second and fourth βαβ domain, and the α-helices in both domains are amphipathic (Fig. 8), although there is no significant homology between the first and third domain (Fig. 8). We propose that the N-terminal domain of the *a*-subunit is a loop with the first and the fourth βαβ domain near the connection to $A_0$ and the second and third on the other side, leaving the mainly α-helical domains between the βαβ domains forming the collar proper. The interaction with the EH peripheral stalks is mediated by the two similar sets of βαβ domains, which may have arisen by a gene duplication. A recent report (66) shows a 1:1:1 complex between the E, H, and $a_N$ equivalents of *E. hirae.* Small angle x-ray scattering experiments showed this complex to be L-shaped with dimensions which fit our model. Moreover, dimerization of E and H as well as interaction of H with $a_N$ is shown, but no interaction of E with $a_N$ in the absence of H. This implies that the interaction of the peripheral stalk with *a* is mediated through the N terminus of H. The only discrepancy between this study and our model is the presence of only one

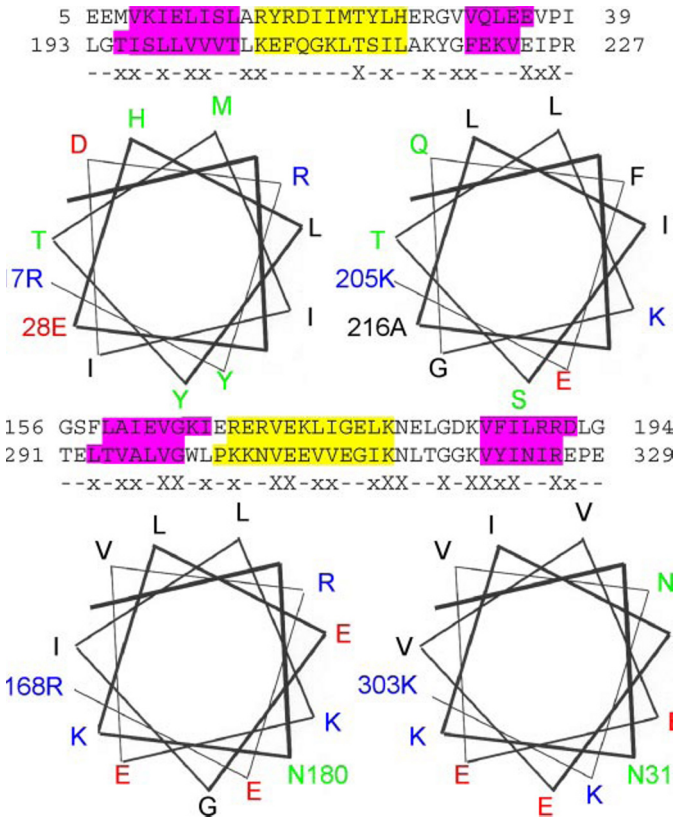


FIGURE 8. **Secondary structure elements of the *P. furiosus* *a*-subunit.** Four regions of the sequence are shown with predicted β-strands in *pink* and α-helices in *yellow*. Identical amino acids between the two sets of regions are indicated with *capital X* and homologous amino acids with *lowercase x*. Helical wheels are shown for the helices with hydrophobic side chains shown in *black*, polar in *green*, positively charged in *blue*, and negatively charged in *red*.

EH dimer in the ternary complex. This may be caused by the absence of the $a_C$ domain and resulting conformational differences.

## DISCUSSION

$A_1A_0$ ATP synthases and $V_1V_0$ ATPases form two distinct groups of enzymes that are related to each other and more distantly to the F-type ATPases. A core group of subunits is highly conserved, whereas others are specific for certain groups. The structures of several subunits have been solved by x-ray crystallography and NMR spectroscopy in the last few years. For the whole enzyme, projections (18, 67, 68) and three-dimensional structures (19–22) by EM are available for several species. Cross-linking experiments have clarified the positions of subunits relative to each other (53, 54, 61, 62). The stoichiometry of the subunits is not yet firmly established. Whereas a consensus is emerging for the structure of the head and the rotor, different models exist for the stator. The eukaryotic $V_1V_0$ ATPases not only have additional subunits and a regulation ($V_1$-$V_0$ dissociation/association) that is not observed in $A_1A_0$, but there are indications that they have a different stator than the prokaryotic enzymes, including possibly a third peripheral stalk.

The $A_1A_0$ ATP synthase from the hyperthermophilic archaeon *P. furiosus* is very suitable for structural investigation because of its high stability. Using the new technique of LILBID analysis, we were able to determine the total molecular weight

and identify all subunits. The high stability made it possible to do a three-dimensional reconstruction, which is the first of an archaeal $A_1A_0$ ATP synthase. The overall structure is very similar to the bacterial A-type ATP synthase from *T. thermophilus* (19) and shows two peripheral stalks, one of which connects to the transmembrane domain. Fitting of the structure of isolated subunits with the total MW as a constraint led us to propose a model for the stator structure where heterodimers of subunits E and H form the peripheral stalks and knobs, both with the C-terminal domains near the head and the N termini forming a coiled coil in the stalk. The N-terminal domain of subunit *a* forms the collar and a topology model for this domain is proposed where two homologous domains interact with each EH dimer.

The *c*-subunit has a conserved sequence across all species in F-, V-, and A-type ATPases. It forms $\alpha$-helical transmembrane hairpins and assembles into rings. The size of the rings is variable in F-type ATP synthases, where rings with 10 (29), 11 (31, 32, 55), 13 (33), 14 (34), and 15 (35) subunits have been identified. In the case of $V_1V_0$ ATPases and $A_1A_0$ ATP synthases structural knowledge is more limited, but there appears to be even more variety. The bacterial V/A-type ATPase from *E. hirae* contains a ring of 10 duplicated subunits with one ion translocation site each, with a total of 20 hairpins (52), whereas the bacterial $A_1A_0$ ring from *T. thermophilus* has 12 single subunits (56). No structural data is available for archaeal *c*-rings, but *M. kandleri* contains a gene coding for a fused 13-hairpin *c*-subunit (26). Other archaea show a variety of duplicated and triplicated fused genes (1), which are not consistent with a tridecameric ring, and occasionally have lost some ion translocating sites. Our LILBID analysis indicates the presence of an $ac_{10}$ subcomplex, and a large $c_{10}$-ring fits the map well. We conclude that the *P. furiosus* ATP synthase has a ring of 10 subunits with 20 hairpins and 10 ion translocation sites. An ATP synthase with a stoichiometry of $A_3B_3CDE_2FH_2ac_{10}$ would have a molecular mass of 738 kDa, fitting well with the mass of 730 $\pm$ 10 kDa as determined by LILBID.

The ability of pyrococci to synthesize ATP with a duplicated *c*-subunit that has lost one ion binding site (39) has been an enigma. F-type ATP synthases have so far been shown to have 10 (29, 32) to 15 (35) ion binding sites in the ring and prokaryotic A-type 10 (52) to 12 (56). The pyrococci would need a *c*-ring with a considerably larger physical size than the F-type ATP synthases to have a sufficient number of ion binding sites, and we have shown that this is the case. According to $\Delta G_p = -n \cdot F \cdot \Delta\mu_{ion}$, a phosphorylation potential ($\Delta G_p$)of ~50 to 70 kJ/mol would be sustained by the use of $n = 2.9-4$ ions/ATP at a physiological electrochemical ion potential of −180 mV ($\Delta\mu_{ion}$) (69). Ten subunits and thus ten ion binding sites in the ATP synthase from *P. furiosus* would give an ion/ATP stoichiometry of 3.3. This would be sufficient to synthesize ATP, providing an explanation for the enigma of ATP synthesis in *P. furiosus*.

*Acknowledgments—We thank Michael Thomm and Harald Huber for supplying cells of P. furiosus, Deryck Mills for assistance with electron microscopy, and Remco Wouts for computational support. We thank Werner Kühlbrandt for support and comments on the manuscript.*

**REFERENCES**

1. Müller, V., and Grüber, G. (2003) *Cell. Mol. Life Sci.* **60,** 474–494
2. Müller, V., Ruppert, C., and Lemker, T. (1999) *J. Bioenerg. Biomembr.* **31,** 15–27
3. Müller, V., Lingl, A., Lewalter, K., and Fritz, M. (2005) *J. Bioenerg. Biomembr.* **37,** 455–460
4. Zimniak, L., Dittrich, P., Gogarten, J. P., Kibak, H., and Taiz, L. (1988) *J. Biol. Chem.* **263,** 9102–9112
5. Bowman, E. J., Tenney, K., and Bowman, B. J. (1988) *J. Biol. Chem.* **263,** 13994–14001
6. Hirata, R., Ohsumi, Y., Nakano, A., Kawasaki, H., Suzuki, K., and Anraku, Y. (1990) *J. Biol. Chem.* **265,** 6726–6733
7. Puopolo, K., Kumamoto, C., Adachi, I., and Forgac, M. (1991) *J. Biol. Chem.* **266,** 24564–24572
8. Grüber, G., Svergun, D. I., Coskun, Ü., Lemker, T., Koch, M. H. J., Schägger, H., and Müller, V. (2001) *Biochemistry* **40,** 1890–1896
9. Coskun, Ü., Grüber, G., Koch, M. H. J., Godovac-Zimmermann, J., Lemker, T., and Müller, V. (2002) *J. Biol. Chem.* **277,** 17327–17333
10. Grüber, G., Wieczorek, H., Harvey, W. R., and Müller, V. (2001) *J. Exp. Biol.* **204,** 2597–2605
11. Maegawa, Y., Morita, H., Iyaguchi, D., Yao, M., Watanabe, N., and Tanaka, I. (2006) *Acta Crystallogr. D Biol. Crystallogr.* **62,** 483–488
12. Schäfer, I. B., Bailer, S. M., Düser, M. G., Börsch, M., Bernal, R. A., Stock, D., and Grüber, G. (2006) *J. Mol. Biol.* **358,** 725–740
13. Lokanath, N. K., Matsuura, Y., Kuroishi, C., Takahashi, N., and Kunishima, N. (2007) *J. Mol. Biol.* **366,** 933–944
14. Iwata, M., Imamura, H., Stambouli, E., Ikeda, C., Tamakoshi, M., Nagata, K., Makyio, H., Hankamer, B., Barber, J., Yoshida, M., Yokoyama, K., and Iwata, S. (2004) *Proc. Natl. Acad. Sci. U. S. A.* **101,** 59–64
15. Numoto, N., Kita, A., and Miki, K. (2004) *Acta Crystallogr. D Biol. Crystallogr.* **60,** 810–815
16. Gayen, S., Vivekanandan, S., Biukovic, G., Grüber, G., and Yoon, H. S. (2007) *Biochemistry* **46,** 11684–11694
17. Biukovic, G., Rössle, M., Gayen, S., Mu, Y., and Grüber, G. (2007) *Biochemistry* **46,** 207–2078
18. Coskun, Ü., Chaban, Y. L., Lingl, A., Müller, V., Keegstra, W., Boekema, E. J., and Grüber, G. (2004) *J. Biol. Chem.* **279,** 38644–38648
19. Bernal, R. A., and Stock, D. (2004) *Structure* **12,** 1789–1798
20. Domgal, I., Venzke, D., Lüttge, U., Ratajczak, R., and Böttcher, B. (2002) *J. Biol. Chem.* **277,** 13115–13121
21. Wilkens, S., Inoue, T., and Forgac, M. (2004) *J. Biol. Chem.* **279,** 41942–42949
22. Gregorini, M., Wang, J., Xie, X.-S., Milligan, R. A., and Engel, A. (2007) *J. Struct. Biol.* **158,** 445–454
23. Coskun, Ü., Radermacher, M., Müller, V., Ruiz, T., and Grüber, G. (2004) *J. Biol. Chem.* **279,** 22759–22764
24. Ruppert, C., Schmid, R., Hedderich, R., and Müller, V. (2006) *FEMS Microbiol. Lett.* **195,** 47–51
25. Fricke, W. F., Seedorf, H., Henne, A., Krüer, M., Liesegang, H., Hedderich, R., Gottschalk, G., and Thauer, R. K. (2006) *J. Bacteriol.* **188,** 642–658
26. Slesarev, A. I., Mezhevaya, K. V., Makarova, K. S., Polushin, N. N., Shcherbinina, O. V., Shakhova, V. V., Belova, G. I., Aravind, L., Natale, D. A., Rogozin, I. B., Tatusov, R. L., Wolf, Y. I., Stetter, K. O., Malykh, A. G., Koonin, E. V., and Kozyavkin, S. A. (2002) *Proc. Natl. Acad. Sci. U. S. A.* **99,** 4644–4649
27. Lolkema, J. S., and Boekema, E. J. (2003) *FEBS Lett.* **543,** 47–50
28. Müller, V. (2004) *J. Bioenerg. Biomembr.* **36,** 115–125
29. Stock, D., Leslie, A. G., and Walker, J. E. (1999) *Science* **286,** 1700–1705
30. Stahlberg, H., Müller, D. J., Suda, K., Fotiadis, D., Engel, A., Meier, T., Matthey, U., and Dimroth, P. (2001) *EMBO Rep.* **2,** 229–233
31. Meier, T., Ferguson, S. A., Cook, G. M., Dimroth, P., and Vonck, J. (2006) *J. Bacteriol.* **188,** 7759–7764
32. Fritz, M., Klyszejko, A. L., Morgner, N., Vonck, J., Brutschy, B., Muller, D. J., Meier, T., and Müller, V. (2008) *FEBS J.* **275,** 1999–2007
33. Meier, T., Morgner, N., Matthies, D., Pogoryelov, D., Keis, S., Cook, G. M., Dimroth, P., and Brutschy, B. (2007) *Mol. Microbiol.* **65,** 1181–1192
34. Seelert, H., Poetsch, A., Dencher, N. A., Engel, A., Stahlberg, H., and Mül-

ler, D. J. (2000) *Nature* **405,** 418–419
35. Pogoryelov, D., Yu, J., Meier, T., Vonck, J., Dimroth, P., and Müller, D. J. (2005) *EMBO Rep.* **6,** 1045–1052
36. Mandel, M., Moriyama, Y., Hulmes, J. D., Pan, Y.-C. E., Nelson, H., and Nelson, N. (1988) *Proc. Natl. Acad. Sci. U. S. A.* **85,** 5521–5524
37. Nelson, N., and Taiz, L. (1989) *Trends Biochem. Sci.* **14,** 113–116
38. Cross, R. L., and Taiz, L. (1990) *FEBS Lett.* **259**
39. Sapra, R., Bagramyan, K., and Adams, M. W. (2003) *Proc. Natl. Acad. Sci. U. S. A.* **100,** 7545–7550
40. Cross, R. L., and Müller, V. (2004) *FEBS Lett.* **576,** 1–4
41. Pisa, K. Y., Huber, H., Thomm, M., and Müller, V. (2007) *FEBS J.* **274,** 2928–2938
42. Bradford, M. M. (1976) *Anal. Biochem.* **72,** 248–254
43. Bode, C., Goebell, H., and Stahler, E. (1968) *Z. Klin. Chem. Klin. Biochem.* **6,** 418–422
44. Morgner, N., Barth, H. D., and Brutschy, B. (2006) *Aust. J. Chem.* **59,** 109–114
45. Morgner, N., Kleinschroth, T., Barth, H. D., Ludwig, B., and Brutschy, B. (2007) *J. Am. Soc. Mass Spectrom.* **18,** 1429–1438
46. Ludtke, S. J., Baldwin, P. R., and Chiu, W. (1999) *J. Struct. Biol.* **128,** 82–97
47. van Heel, M., Harauz, G., Orlova, E. V., Schmidt, R., and Schatz, M. (1996) *J. Struct. Biol.* **116,** 17–24
48. Pettersen, E. F., Goddard, T. D., Huang, C. C., Couch, G. S., Greenblatt, D. M., Meng, E. C., and Ferrin, T. E. (2004) *J. Comput. Chem.* **25,** 1605–1612
49. Maeder, D. L., Weiss, R. B., Dunn, D. M., Cherry, J. L., Gonzalez, J. M., DiRuggiero, J., and Robb, F. T. (1999) *Genetics* **152,** 1299–1305
50. Morgner, N., Hoffmann, J., Barth, H. D., Meier, T., and Brutschy, B. (2008) *Int. J. Mass Spectr.* **277,** 309–313
51. Morgner, N., Zickermann, V., Kerscher, S., Wittig, I., Abdrakhmanova, A., Barth, H.-D., Brutschy, B., and Brandt, U. (2008) *BBA-Bioenergetics* **1777,** 1384–1391
52. Murata, T., Yamato, I., Kakinuma, Y., Leslie, A. G. W., and Walker, J. E. (2005) *Science* **308,** 654–658
53. Arata, Y., Baleja, J. D., and Forgac, M. (2002) *Biochemistry* **41,** 11401–11407
54. Xu, T., Vasilyeva, E., and Forgac, M. (1999) *J. Biol. Chem.* **274,** 28909–28915
55. Vonck, J., Krug von Nidda, T., Meier, T., Matthey, U., Mills, D. J., Kühlbrandt, W., and Dimroth, P. (2002) *J. Mol. Biol.* **321,** 307–316
56. Toei, M., Gerle, C., Nakano, M., Tani, K., Gyobu, N., Tamakoshi, M., Sone, N., Yoshida, M., Fujiyoshi, Y., Mitsuoka, K., and Yokoyama, K. (2007) *Proc. Natl. Acad. Sci. U. S. A.* **104,** 20256–20261
57. Meier, T., Polzer, P., Diederichs, K., Welte, W., and Dimroth, P. (2005) *Science* **308,** 659–662
58. Stocker, A., Keis, S., Vonck, J., Cook, G. M., and Dimroth, P. (2007) *Structure* **15,** 904–914
59. Jones, D. T. (1999) *J. Mol. Biol.* **292,** 195–202
60. Bryson, K., McGuffin, L. J., Marsden, R. L., Ward, J. J., Sodhi, J. S., and Jones, D. T. (2005) *Nucleic Acids Res.* **33,** W36–38
61. Schäfer, I., Rössle, M., Biukovic, G., Müller, V., and Grüber, G. (2006) *J. Bioenerg. Biomembr.* **38,** 83–92
62. Arata, Y., Baleja, J. D., and Forgac, M. (2002) *J. Biol. Chem.* **277,** 3357–3363
63. Kish-Trier, E., Briere, L.-A., Dunn, C. D., and Wilkens, S. (2008) *J. Mol. Biol.* **375,** 673–685
64. Esteban, O., Bernal, R. A., Donohoe, M., Videler, H., Sharon, M., Robinson, C. V., and Stock, D. (2008) *J. Biol. Chem.* **283,** 2529–2603
65. Wilkens, S., and Forgac, M. (2004) *J. Biol. Chem.* **276,** 44064–44068
66. Yamamoto, M., Unzai, S., Saijo, S., Ito, K., Mizutani, K., Suno-Ikeda, C., Yabuki-Miyata, Y., Terada, T., Toyama, M., Shirouzu, M., Kobayashi, T., Kakinuma, Y., Yamato, I., Yokoyama, S., Iwata, S., and Murata, T. (2008) *J. Biol. Chem.* **283,** 19422–19431
67. Boekema, E. J., van Breemen, J. F., Brisson, A., Ubbink-Kok, T., Konings, W. N., and Lolkema, J. S. (1999) *Nature* **401,** 37–38
68. Ubbink-Kok, T., Boekema, E. J., van Breemen, J. F. L., Brisson, A., Konings, W. N., and Lolkema, J. S. (2000) *J. Mol. Biol.* **296,** 311–321
69. Schäfer, G., Engelhard, M., and Müller, V. (1999) *Microbiol. Mol. Biol. Rev.* **63,** 570–620